Lattice dynamics of silicon nanostructures

To cite this article: S P Hepplestone and G P Srivastava 2006 *Nanotechnology* **17** 3288

INSTITUTE OF PHYSICS PUBLISHING NANOTECHNOLOGY
Nanotechnology **17** (2006) 3288–3298 doi:10.1088/0957-4484/17/13/035

Lattice dynamics of silicon nanostructures

S P Hepplestone and G P Srivastava

School of Physics, University of Exeter, Stocker Road, Exeter EX4 4QL, UK

Received 30 January 2006
Published 12 June 2006
Online at stacks.iop.org/Nano/17/3288

Abstract
The lattice dynamical results of silicon nanostructures with all three different degrees of confinement (nanoslabs, nanowires, nanodots) are systematically analysed and presented using an adiabatic bond charge model. In the direction of propagation of these structures, it is found that the phonon branches change from flat, for the smallest nanostructures, to dispersive as the nanostructure size increases. It is also noted that in the direction of confinement all but the acoustic branches are generally flat, with very little dispersion. The trends in the variations of the lowest and highest confined modes at the Brillouin zone centre with nanostructure size are investigated. In particular, analytic expressions for the size variation of the highest mode with the dimensionality of the nanostructures have been presented. Also, an analytic fit has been presented for the size variation of the lowest non-zero acoustic mode with structure size. Finally, numerical calculations based upon Fermi's Golden Rule formula of the dependence of the lifetime of the lowest confined mode on nanostructure size and temperature have also been obtained and discussed.

(Some figures in this article are in colour only in the electronic version)

1. Introduction

In the last decade several types of nanostructure (such as nanowires, nanodots, nanorings, ultrathin films or nanoslabs, and nanotubes) have been grown and identified [1–8]. These nanostructures occur in two forms: stand alone and grown upon substrate. Structures such as these are considered to be the building blocks of components for future electronic devices [9]. The applications of these nanostructures in potential future devices are heavily dependent on their electronic, optical and thermal properties. Whilst the electronic properties of such nanostructures are very well studied [10–13] and are still an active area of research, their thermal properties have received comparatively less attention [14–16]. The thermal properties of materials, in particular of semiconducting systems, are almost entirely governed by phonons, their dispersion relations and their interactions. The phonon dispersion relations in nanostructures are expected to be significantly different from the bulk due to the confinement effects such systems offer. It is very important, therefore, to acquire adequate knowledge of phonon dispersion relations in nanostructures, and the lifetimes of the confined phonon modes.

The phonon dispersion relations in low dimensional systems have been studied using several different methods for the last 25 years or so. These can be broadly classified as continuum models and lattice dynamical models. The continuum models have been employed to describe the phonon dispersion of nanostructures since the early 1990s, when Stroscio *et al* [10, 11, 17] used an elastic continuum model to investigate the lattice dynamics of the acoustic modes of nanodots, nanoslabs and nanowires (both cylindrical and rectangular). A good discussion of these models is presented by Stroscio and Dutta [10]. Lattice dynamical models of different sophistication have been employed to describe the phonon dispersion in nanostructures since the early 1980s. In particular, during the 1980s, nanoslabs received considerable attention [18]. It is not until the last decade that calculations began to been performed for nanodots (microcrystals) [19] and nanowires [15]. None of these works has provided a full and detailed discussion of the lattice dynamics of nanostructures. However, in these works, two zone-centre modes have been of considerable interest: the highest optical mode and the lowest non-zero mode.

Stroscio *et al* [10, 11, 17] used an elastic continuum model to investigate the phonon dispersion of the acoustic modes of both cylindrical and rectangular nanowires. This approach provided information on one acoustic branch (the dilatational mode) and a qualitative description of phonon dispersion in realizable-size quantum dots and wires. Also, this model

provided information about a new lowest non-zero zone-centre mode, which is produced due to confinement effects and lies in the acoustic range. Hereon, we will consider this mode to have the frequency ω_σ. In 1997 Nishiguchi *et al* [14] used a variational model to discern the nature of the acoustic modes in nanowires. Using this model, Nishiguchi *et al* predicted the existence of four acoustic branches and calculated their dispersion relations. However, due to the focused nature of this technique, they were unable to yield a full set of phonon dispersion curves for nanowires. In 2003 Mingo *et al* [15] used a force constant model with frozen boundary conditions to obtain the full phonon dispersions of an ultrathin nanowire grown in the [110] direction. In a more recent work, Mingo *et al* [20] used an atomistic Green's function approach (with completely reflective boundaries) to calculate the phonon dispersion of ultrathin wires. These two recent techniques show strong agreement in the optical region of the phonon dispersion curves, but the former technique does not yield a fourth acoustic mode obtained by Nishiguchi *et al*. More recently Thonhauser *et al* [21] used a simple spring and mass model to discuss whether clamped or free standing boundary conditions are appropriate to calculate phonon modes in a nanowire grown in the [111] direction. In this work they concluded that for optical modes it is more appropriate to consider clamped boundary conditions. Their work also confirmed the presence of four acoustic modes obtained in the work of Nishiguchi *et al*. However, this work did not investigate variations of phonon modes with nanowire size.

For nanoslabs, long wavelength optical modes were obtained on the basis of a very simple valence force field model in 1980 by Kanellis *et al* [18]. They showed using this simple technique for thin slabs that the frequency of the highest optical mode is lower than the corresponding bulk case, rising almost exponentially towards the bulk value with increasing slab thickness. In contrast, Jusserand *et al* [22] suggested using a simple theory based upon the diatomic linear chain model that the confined zone-centre highest optical mode ω_{optical} varies as $\omega^2_{\text{optical}} - \omega^2_{\text{bulk}} \propto 1/d^2$, where d is the thickness of the slab. This result applies to both slabs and superlattices. Nanoslabs are also characterized by the presence of the lowest non-zero zone-centre acoustic mode of frequency ω_σ. The variation of this mode with slab thickness has traditionally been described with Lamb's theory [23, 24].

For nanodots and microcrystals, the variation of confined acoustic and optical modes with the size of the system has been discussed using several theories, without a general consensus being reached. A good review of these variations has recently been presented by Sun *et al* [25]. Continuum theories have been applied to nanodots to predict their phonon dispersion, and the variation of the confined modes with the size of the structure. These theories, however, are inapplicable for ultrasmall structures (typically for sizes smaller than 15 Å).

As discussed above, despite some work being carried out, there is in general lack of a comprehensive theory of the lattice dynamics of nanostructures. No single technique has been applied to investigate similar features in different nanostructures, making comparison unreliable. More importantly, with existing available methods it is not possible to identify which important features are dependent on dimensionality and which are dependent on the size of the nanostructure, or possibly whether both factors contribute to such features.

Previously, we have presented preliminary results for the lattice dynamics of stand-alone nanowires [26] and a brief report on the lattice dynamics of simple stand-alone nanostructures [27] highlighting some key features. In this paper we present a systematic study of the lattice dynamics of silicon nanostructures (nanoslabs, nanowires, nanodots and nanowires upon substrate) using the well established adiabatic bond charge model developed by Weber [28]. We also present lifetime calculations of the lowest non-zero zone-centre mode of frequency ω_σ for these structures. In section 2.1 we introduce our implementation of the theory for studying four different types of nanostructure: stand-alone nanoslabs, stand-alone nanowires, stand-alone nanodots and nanowires grown upon a nanoslab. In section 2.2 we present our approach for the calculation of the lifetime of the ω_σ mode in the silicon nanostructures using the calculated phonon dispersion relations and time dependent perturbation theory. In section 3 we present results of our calculations for the lattice dynamics of silicon nanostructures, in which we contrast and compare some common features of such systems and also show the features which are unique to each particular nanostructure. We also present lifetime results for the ω_σ mode for the different nanostructures presented and for different sizes of stand-alone nanowires. Finally, in section 4 we present our conclusions.

2. Methodology

2.1. Theoretical modelling of silicon nanostructure lattice dynamics

The adiabatic bond charge method was originally developed by Weber [28] in 1977 for studying the lattice dynamics of tetrahedrally bonded bulk semiconductors. The valence charge density is considered as point charges, called bond charges (bcs), located midway along the tetrahedral bonds between nearest homopolar neighbours. These bond charges are allowed to move adiabatically and are assumed to have zero mass. The equations of motion for the ions and their bond charges are evaluated and a dynamical matrix is obtained by considering three types of interaction: (i) Coulomb interaction between all particles within the structure (ion–ion, ion–bc, bc–bc), which is evaluated using the Ewald summation technique, (ii) short range central force interaction acting centrally between nearest neighbours (ion–ion, ion–bc, bc–bc), and (iii) a rotationally invariant Keating type bond bending interaction [29], depending on the bc–ion–bc angle. Once these interactions are taken into account, dispersion relations of the form $\omega = \omega(\mathbf{q})$ are obtained for the lattice dynamics of the system.

We applied this approach to five different system types without a change in methodology or introducing new variables or simplifications: three-dimensional bulk (3D) silicon; periodic silicon supercells in the form of quasi-two-dimensional nanoslabs (2D) with thickness d; quasi-one-dimensional nanowires (1D) with dimensions $d \times d$; quasi-zero-dimensional nanodots (0D) with square cross-sections of dimensions $d \times d \times d$; and quasi-one-dimensional nanowires grown upon a quasi-two-dimensional nanoslab. The nanoslab

layers are made of Si(001) bi-layers, and the nanowire axis is also along [001]. The nanostructures were modelled within the supercell geometry, constructed with an artificial periodic arrangement invoked. Neighbouring nanostructures were separated by a vacuum region large enough to prevent interactions between them, but not oversized to maximize computational efficiency. Such a scheme has been successfully applied to study the lattice dynamics of semiconductor surfaces (see, e.g. [30, 31]).

The vacuum region was considered to consist of an embedding material with the same atomic network as the nanostructure, but with atomic mass less than 10^{-6} of a single silicon atom. With this simple consideration the nanostructure retains its unreconstructed geometry at its interface with the vacuum, and the dangling bonds at the surface(s) remain in their bulk positions. Thus the silicon bulk parameters for the adiabatic bond charge model are employed without any alteration. The phonon frequencies due to the embedding material lie far above the frequency regions for the bulk and nanostructure, and are easily discarded from the analysis of results. The in-plane periodicity for nanoslabs and along-axis periodicity for nanowires avoid the problem of determining complex phonon frequencies which may arise due to finite length of the system.

Our embedding technique, which *almost* mimics the clamped boundary conditions employed by Thonhauser *et al* is expected to produce a good description of the physics of atomic vibrations in nanostructures, but would not allow for four acoustic branches obtained for free standing nanowires [14]. We chose the embedding technique deliberately, as practical considerations of uses of nanostructures mean these structures will be fixed to an additional system (normally a bulk substrate, or in the case of nanowires, suspended and connecting two bulk-like systems), which is expected to prevent the existence of the torsional mode. An ultralight mass was chosen as opposed to an infinite mass because the latter choice leads to an interference between the vibrational spectral of the embedding medium and the sample. An additional advantage of the ultralight mass embedding technique is that when the embedding mass replaced by hydrogen mass, we can obtain results for hydrogenated surfaces.

An optimum amount of the vacuum region was chosen within the computational resources available to us. For our calculations presented here, all results have been carried out with a vacuum region of 1.086 nm between neighbouring supercells, except for the 3.8 nm × 3.8 nm nanowire and the 1.62 nm × 1.62 nm × 1.62 nm dot, where due to computation limitations the vacuum was set to be 0.543 nm (i.e. equivalent to the bulk lattice constant). Within our supercell approach, phonon branches in the direction of confinement exhibit slight dispersive tendencies. This is due to two factors: (i) the *quasi-2D/1D/0D* nature of these systems and (ii) the interaction between neighbouring unit cells. For a vacuum size of 1.086 nm between neighbouring supercells, we estimate a maximum inaccuracy of 1 cm^{-1} for optical modes and 10 cm^{-1} for low-lying non-zero zone-centre modes. The error is less in the optical region, where maximum inaccuracy for a vacuum of 0.543 nm was 3 cm^{-1}. This is well within experimental errors of measurements of such modes. For example, for a nanowire with a width of $d = 0.543$ nm, vacuum regions of 0.543, 1.629 and 3.801 nm produced results for the highest optical mode to be 480.56, 477.51 and 477.14 cm^{-1}, respectively.

For all the modelled nanostructures we will consider Γ–X, Γ–Y and Γ–Z as the principal symmetry directions in the Brillouin zone. For nanoslabs Γ–X will be considered the direction of confinement. For nanowires confining directions will be considered as Γ–X and Γ–Y. For nanodots phonons are confined along all the three symmetry directions. For the nanowire upon a substrate, Γ–Z is the direction of propagation in both the wire and the slab, Γ–Y is considered to be perpendicular to the wire, but parallel to the surface, and Γ–X is the direction perpendicular to the slab and the wire.

2.2. Lifetime calculations

Once the dispersion relation $\omega = \omega_s(\mathbf{q})$ is known, it would be useful to determine the intrinsic lifetime of some important zone-centre modes, assuming they are populated over their Bose–Einstein equilibrium distribution $\bar{n}(\omega)$. In order to calculate the intrinsic lifetime of the lowest non-zero mode in clamped nanostructures we first determine if these systems should be treated as quasi-one-dimensional or three-dimensional. To do this we examine the wavelength of the dominant phonon mode over a range of temperatures. The energy $\hbar\omega_{\mathrm{dom}}$ of the dominant phonon mode in a D-dimensional solid is obtained by maximizing the expression [32]

$$g^D(\omega)\bar{n}(\bar{n}+1), \tag{1}$$

where $g^D(\omega)$ is the density of phonon states in the D-dimensional solid, and $\bar{n} \equiv \bar{n}(\omega)$ is the Bose–Einstein distribution function. Assuming the validity of the continuum model (with linear dispersion) for low-lying acoustic modes, we note that $g^D(\omega) \propto \omega^{D-1}$. With this choice for $g^D(\omega)$, it can shown that the dominant mode has the energy $\hbar\omega_{\mathrm{dom}} = \alpha kT$, where α is 1.6 and ∞ for three- and one-dimensional solids, respectively. This implies that for a one-dimensional solid the dominant phonon wavelength will be infinitely small. Therefore, for the dominant phonon mode in any system with a non-zero width (quasi-confined) will appear to be three-dimensional. However, it also implies that the wavelength of the dominant phonon mode for a three-dimensional solid becomes greater than the lateral size of a nanowire or a nanotube below a certain temperature. This typically happens below 50 K for clamped silicon nanostructures. With this in mind, we have modelled the nanostructures as three-dimensional systems and have presented results for temperatures above 50 K.

The decay time of a phonon in mode $\mathbf{q}s$ (with wavevector $\mathbf{q}$ and polarization index s) via a three-phonon process due to cubic anharmonicity in the crystal potential into two lower energy phonon modes $\mathbf{q}'s'$ and $\mathbf{q}''s''$ can be expressed as [32, 33]

$$\tau_{\mathbf{q}s}^{-1} = \frac{1}{2\bar{n}(\bar{n}+1)} \sum_{\mathbf{q}',\mathbf{q}''} \sum_{s',s''} \bar{P}_{\mathbf{q}s}^{\mathbf{q}'s',\mathbf{q}''s''}, \tag{2}$$

where $\bar{P}$ denotes the equilibrium transition probability for a decay process. We have considered the cubic anharmonicity in the framework of an anharmonic elastic continuum [33]. With the application of Fermi's golden rule formula, for a Normal

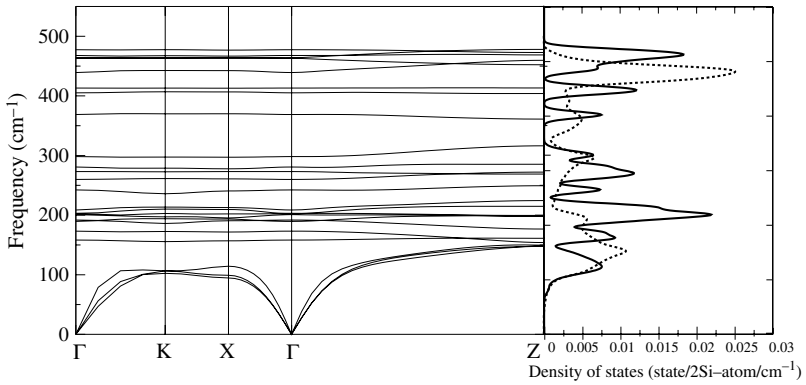

Figure 1. The phonon dispersion curves and density of states for a silicon nanowire of cross section 0.543 nm × 0.543 nm. The Γ–X direction is considered to be perpendicular to the direction of propagation of the wire, the Γ–Z direction is parallel to the direction of propagation of the wire, and Γ–K is along the face diagonal in the Brillouin zone for the wire. Also shown are the density of states for the wire (bold line) and the density of states of bulk silicon (dashed line).

process characterized with $\mathbf{q} = \mathbf{q}' + \mathbf{q}''$, equation (2) can be re-expressed as

$$\tau_{\mathbf{q}s}^{-1} = \frac{\pi\gamma^2\hbar}{2\rho\bar{c}^2V}\sum_{\mathbf{q}',\mathbf{q}''}\sum_{s',s''}\omega(\mathbf{q}s)\omega(\mathbf{q}'s')\omega(\mathbf{q}''s'')\frac{\bar{n}_{\mathbf{q}'s'}\bar{n}_{\mathbf{q}''s''}}{\bar{n}_{\mathbf{q}s}} \delta_{\mathbf{q},\mathbf{q}'+\mathbf{q}''}\delta(\omega(\mathbf{q}s) - \omega(\mathbf{q}'s') - \omega(\mathbf{q}''s'')), \tag{3}$$

where the Grüneisen's constant γ is a measure of cubic anharmonicity, ρ is mass density, $\bar{c}$ is average acoustic phonon speed, and V is crystal volume. Within Debye's isotropic continuum model for acoustic phonon branches, and using the energy and momentum conservation conditions for a zone-centre lowest non-zero phonon mode ($\mathbf{q} = 0$) the above equation yields the following expression for the decay time of such a mode:

$$\tau^{-1} = \frac{\gamma^2\hbar}{4\pi\rho\bar{c}^2}\sum_{s',s''}c_{s'}c_{s''}\frac{\omega_\sigma^5}{(c_{s'}+c_{s''})^5}\frac{\bar{n}'\bar{n}''}{\bar{n}}, \tag{4}$$

where $\bar{n}' = \bar{n}(\omega_\sigma c_{s'}/\{c_{s'}+c_{s''}\})$ and $\bar{n}'' = \bar{n}(\omega_\sigma c_{s''}/\{c_{s'}+c_{s''}\})$.

3. Results and discussion

3.1. Stand-alone nanowires

Phonon dispersion curves were calculated for stand-alone silicon nanowires of cross-section $d \times d$, with d ranging from 0.543 nm (namely $d = a$, the bulk lattice constant) up to 3.801 nm (namely $d = 7a$). In general, two important features were noted in the dispersion curves and density of states (DOS) curves: folding effects (i.e. bulk results folded on to the nanowire Brillouin zone) and confinement effects (i.e. phonon modes which arise due to reduced dimensionality upon the formation of wires).

As can be observed in figure 1, the ultrathin nanowire (the thinnest considered −0.543 nm × 0.543 nm) shows several unusual and unique properties, not seen in thicker nanowires. All the non-acoustic modes are almost flat and dispersionless, even in the direction of propagation, Γ–Z. The acoustic modes have very high group velocities near the zone centre in the Γ–Z direction, nearly three times greater than the corresponding velocities in bulk silicon. Another feature of note is the appearance of several gaps in the DOS. These gaps are located both within and above the bulk silicon acoustic range. Also, within the DOS there are sharp delta-like peaks, showing that for the thinnest nanowire strong quantization effects dominate above all other factors in its phonon dispersion properties. These results show that the ultrathin nanowire is unlike thicker nanowires (as shown in figure 2) and should be treated as a new material with very different properties.

As the wire thickness increases, the gaps in the DOS decrease rapidly. Figure 2 shows clearly that for the nanowire of dimensions greater than 1.08 nm × 1.08 nm (i.e. for $d = 2a$) there are no gaps in the DOS. Also, the peaks broaden and their relative heights change. With increase in the wire thickness the DOS begins to look more like that for bulk silicon. However, as can be clearly seen in the boxed region, in the lower acoustic range that the DOS increases in flat steps. This feature is in strong agreement with the prediction of the Debye continuum model prediction corresponding to $\omega \propto q$ and $g(\omega) \propto \omega^0$. The position of the highest-lying peak in the DOS shifts gradually upwards with the thickness of the nanowire, tending towards the bulk peak for $d > 3a$ as shown in figure 2. The energy of the highest optical mode is shifted downwards due to quantization. The trend in the shift of the highest mode is discussed later in this work. Also, the optical modes slowly become more dispersive in the Γ–Z direction as the wire thickness increases, showing that quantization is less strong for thicker wires as expected. However, in the directions of confinement, these modes remain almost completely flattened for all thicknesses of the wire considered in this work, which indicates minimal interaction between nanostructures.

Another feature that changes as the wire thickness decreases is the group velocity near the zone centre of the dilatational acoustic mode in the direction of propagation (Γ–Z). For the ultrathin nanowires considered here, the group velocity is much higher than in bulk silicon. With an increase in wire thickness the group velocity decreases and drops below the longitudinal bulk value. This shows a clear difference from the results obtained from the continuum model [10] which predicts a constant group velocity which is much lower than bulk for nanowires regardless of thickness. Our results clearly

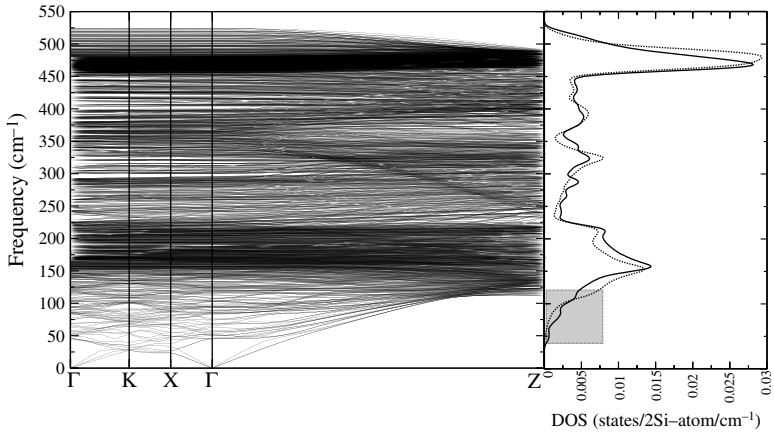

Figure 2. The phonon dispersion curves and density of states for a silicon nanowire of cross section 3.8 nm × 3.8 nm. Also shown are the density of states for the wire (bold line) and the density of states of bulk silicon (dashed line).

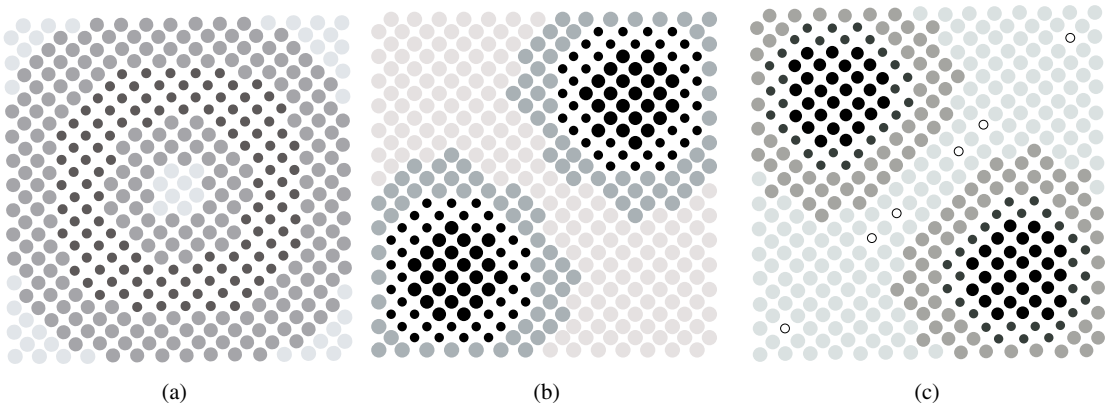

Figure 3. The amplitude of atomic vibration of the three lowest non-zero modes near the zone centre for a nanowire of cross section 3.8 nm × 3.8 nm. The darker the atom, the higher its relative amplitude of vibration compared to other atoms: (a) lowest non-zero mode, (b) second lowest non-zero mode, (c) third lowest non-zero mode.

suggest that with the increase in the system size, the group velocity will decrease towards the result obtained from the continuum model. We hope that our predictions would be confirmed by first-principles calculations.

For thicker wires, lower-lying optical branches are no longer flat or dispersionless, but have non-zero group velocity. For the lowest three optical modes, the amplitudes of atomic vibrations near the zone centre are shown in figure 3 for a nanowire of size 3.8 nm × 3.8 nm (i.e. for $d = 7a$). It can be seen that the upper two of these modes are degenerate in pattern and energy. These three modes are all mixed modes, with partially transverse and partially longitudinal character in atomic vibrations. In particular, the lowest mode is majority transverse-like in its vibrational character and the other two degenerate modes are majority longitudinal-like in character. These modes become increasingly mixed as they change from the Brillouin zone centre (Γ point) to the zone edges (X, Y and Z). The low-lying optical modes in the thinnest nanowire also show mixed polarization behaviour. Although these low-lying optical modes may play an important role in electron–phonon interaction, the lowest of these, the ω_σ mode, is of particular interest. Figure 4 shows the variation of the energy of this mode with the thickness d of the nanowire. This variation can

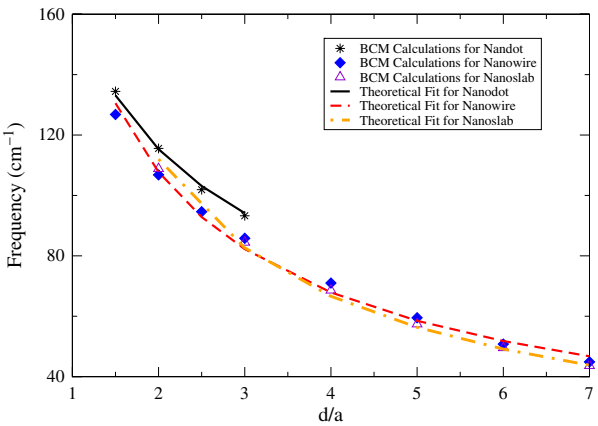

Figure 4. The variation of the lowest non-zero mode ω_σ with the size d of the nanostructure.

be expressed as

$$\omega_\sigma = \frac{A}{d^\alpha}, \tag{5}$$

where α is equal to $2/3 \pm 0.06$ and the proportionality constant

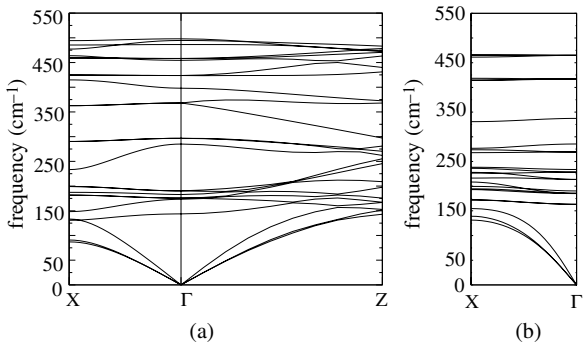

Figure 5. The phonon dispersion curves for (a) a silicon nanoslab of thickness 0.543 nm; (b) a silicon nanodot of size 0.543 nm × 0.543 nm × 0.543 nm.

A is estimated as 3.41 nm$^{2/3}$ THz. It can be clearly seen from the results of the continuum model [10] that this theory predicts $\alpha = 1$. This difference is believed to be a result of the simplistic 1D nature of such a model. It can be seen that using the relationship between ω_σ and d in equation (5) it is straightforward to determine the confining size of a silicon nanowire from Raman scattering measurements. However, it is important to note that this mode will be lowered by amorphous silicon that coats many wires [20, 33].

3.2. Stand-alone nanodots and nanoslabs

Vibrational properties of silicon nanodots and nanoslabs share many common features with nanowires, but also show distinct differences. Nanodots offer confinement in all three directions and as such provide no direction of propagation. Indeed for silicon nanodots the phonon dispersion curves are flat and dispersionless in all directions for all sizes considered here (up to $d = 3a = 1.68$ nm in width), as shown in figure 5(b). This is similar to what is observed in the directions of confinement for nanowires. In the thinnest silicon nanoslab the phonon branches are flat and dispersionless in the direction of confinement, though not to the same degree as for the thinnest nanowire, as shown in figure 5(a). As the size of confinement d increases, it can be seen that the nanodots show much greater flatness in their branches than a nanowire of the same size of confinement. This is not unexpected as there is no direction of propagation for the nanodot, and thus quantization effects completely dominate. Phonon branches remain rather flat for slab thickness $d = 2a = 1.08$ nm and begin to exhibit dispersive behaviour for thicker slabs. However, unlike the ultrathin nanowire or ultrasmall nanodot, the ultrathin nanoslab does not show flatness in the direction of propagation for many of its branches. This is a direct result of a nanoslab only having one degree of confinement as opposed to the nanowires with two degrees of confinement. Thicker nanoslabs show much less flatness in their branches, even in the direction of confinement as size increases.

One other common feature, shown in figure 6, between nanowires, nanodots and nanoslabs is the appearance of several gaps in the DOS in the ultrathin nanostructures. There is a single gap in the DOS, for nanoslabs, observed near 400 cm^{-1}, whereas for the nanowire there are three clear gaps and for the nanodot there are four clear gaps. The number and width of gaps reduce rapidly as the nanostructure size increases and are thus a unique feature of ultrasmall silicon nanostructures. These gaps are observed in the DOS for dots smaller than 1.629 nm × 1.629 nm × 1.629 nm in size, and for wires smaller than 1.086 nm × 1.086 nm. A closer examination of figure 6(b) and the highlighted regions in figures 2 and 6(c) shows that the DOS in the acoustic region follows the prediction of the Debye continuum model (i.e. $g(\omega) \propto \omega$, $g(\omega) \propto \omega^0$, and $g(\omega) \propto \omega^{-1}$, for 2D, 1D and 0D systems, respectively) before becoming bulk-like for much larger systems. This range becomes smaller with increase in the number of degrees of confinement, such that dots become characterized with bulk-like features even for a cubic length of 1.6 nm.

Table 1. The zone-centre lowest non-zero mode for different sizes and dimensionality of nanostructure.

Dimensionality	Size of confinement, d (nm)	ω_σ (cm^{-1})
2	1.68	84.46
2	1.09	108.84
2	0.54	143.69
1	1.68	80.21
1	1.09	103.46
1	0.54	158.22
0	1.68	91.20
0	1.09	119.94
0	0.54	163.29

For the ultrathin nanoslab the group velocity of the fastest acoustic mode is higher in the Γ–Z direction than in bulk, as observed for the ultrathin wire. However, similar to the wire, as the slab thickness increases, the group velocity of this mode near the zone centre decreases to below the bulk value. This change-over occurs for the wire at $d = 3$ nm and for the nanoslab at $d = 16.29$ nm. The velocity of this mode in the nanoslab tends to the bulk value for infinite thickness as expected.

The effect of increased quantization is reflected in the behaviour of the zone-centre lowest non-zero mode ω_σ, as shown in table 1. As the number of degrees of confinement increases, the energy level of ω_σ increases. This is expected as quantization effects increase from nanoslab (2D) to nanowire (1D) to nanodot (0D) due to the increased number of degrees of confinement. This raises the question regarding the behaviour of this mode as a function of d in these structures. Our lattice dynamical results suggest the variation of ω_σ with nanosize in the form in equation (5) with α equal to $3/4 \pm 0.04$ for nanoslabs and $1/2 \pm 0.08$ for nanodots. An interesting observation is that the exponent α can be expressed as $(4 - N)/(5 - N)$, where N is the number of degrees of confinement. The variation of ω_σ with nanosize is shown in figure 4 where the proportionality constant A is obtained to be 3.57 nm$^{3/4}$ THz for nanoslabs and 3.60 nm$^{1/2}$ THz for nanodots. Again, this equation can help identify the confining size of a nanostructure. The above expression agrees with the experimental Raman measurements carried out by Fujii *et al* [34] for the lowest non-zero mode after allowing for an appropriate lowering of the frequency due to the embedding material in their work. It is interesting to note that our lattice dynamical calculations indicate that the size variation of the ω_σ mode is different from that presented from continuum Lamb theory.

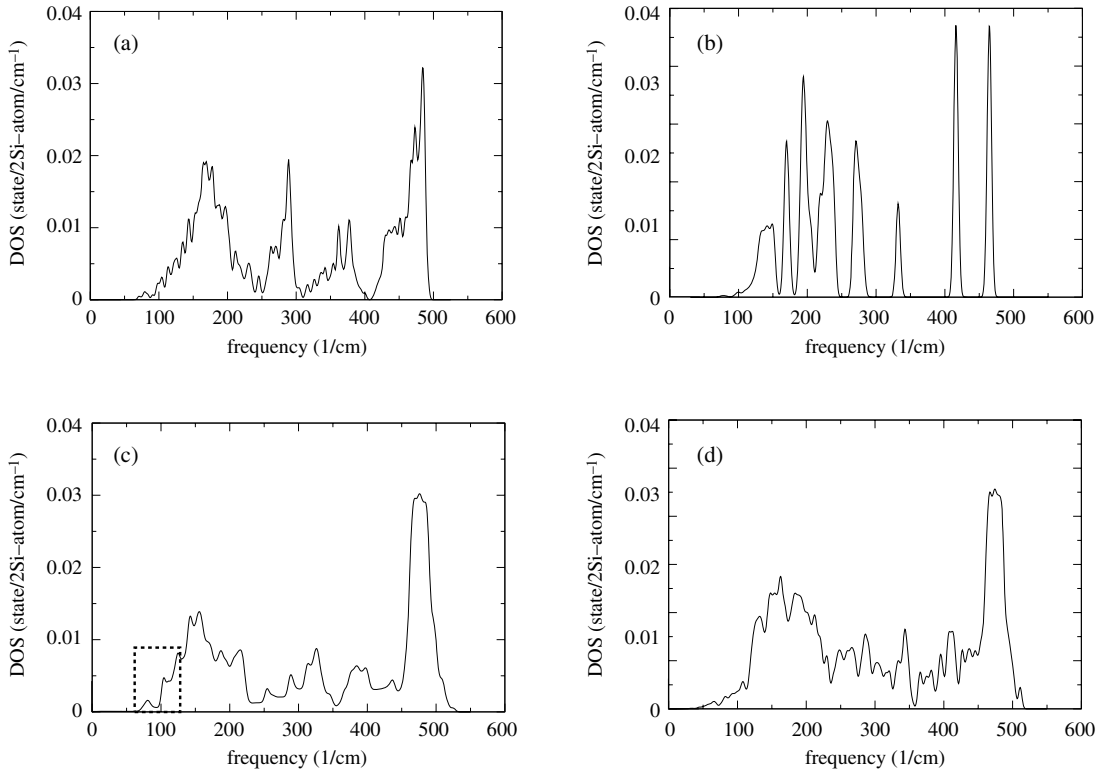

Figure 6. The density of states for thin nanoslabs, square nanowires and cubic nanodots of varying size: (a) nanoslab 0.543 nm thick, (b) nanodot 0.543 nm × 0.543 nm × 0.543 nm in volume, (c) nanoslab 32.520 nm thick, (d) nanodot 1.629 nm × 1.629 nm × 1.629 nm in volume. Continuum-like behaviour is highlighted.

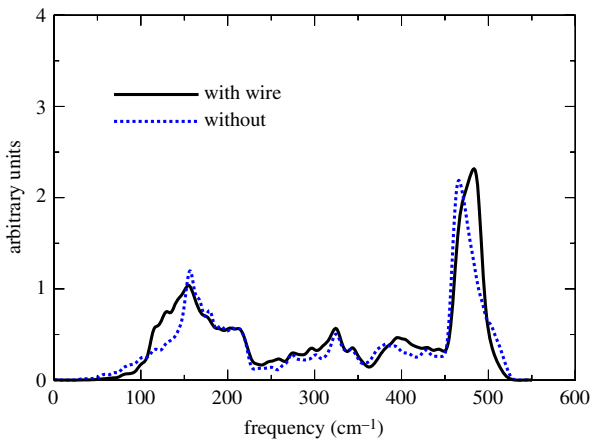

Figure 7. The density of states for a silicon nanoslab of thickness 2.715 nm with and without a nanowire of cross section 0.543 nm × 0.543 nm grown upon it.

3.3. Nanowires on (001) thin substrate

The first expected feature of nanowires on a substrate is a reduction confinement effect phonon spectrum. This is found in present calculations and shown in figure 8. This effect can also be observed in figure 7 which shows the DOS of the ultrathin nanowire on a silicon substrate, compared to an identical slab of silicon substrate without the wire. The DOS in the acoustic range (less than 150 cm^{-1}) shows a step-like behaviour for the wire upon substrate, whereas the DOS for the wireless slab shows linear jumps. These behaviours can be regarded as 1D and 2D respectively, indicating the addition of a wire has a noticeable effect on the DOS of the combined system. Also, the DOS for the slab with a wire grown upon it shows a broader early DOS than the wireless slab. This is because of the introduction of quantized modes in the wire which have low energy. It is also noted that the optical range does not change much between the two systems, suggesting that optical modes will be dominated by bulk effects and low-lying energy modes are dominated by the quantized states that are introduced by the wire.

Figure 8 shows the typical dispersion curves of an ultrathin nanowire on a thin silicon substrate. The upper range of the dispersion curves shows that the optical modes are flattened, suggesting that the optical modes are far more affected by the wire on the substrate than the acoustic modes. It can be seen clearly in all directions that the system has dispersive modes in the range 0 cm^{-1} to approximately 480 cm^{-1}. However, the ω_σ mode is lowered more than in the slab on its own, and much lower than in a ultrathin nanowire. This suggests that the key factor in determining the dependence of the lowest mode is the combined thickness of the substrate and the wire.

Table 2 presents results for ω_σ and the highest optical mode for different thicknesses of the substrate and wire. We find that, for slab thicknesses of 3.801 nm and greater, the value of ω_σ saturates to a constant value of approximately 40 cm^{-1}. For thicker wires upon a given thickness of the substrate a similar trend was observed, but firm conclusions cannot be reached due to computational limitations. Similarly,

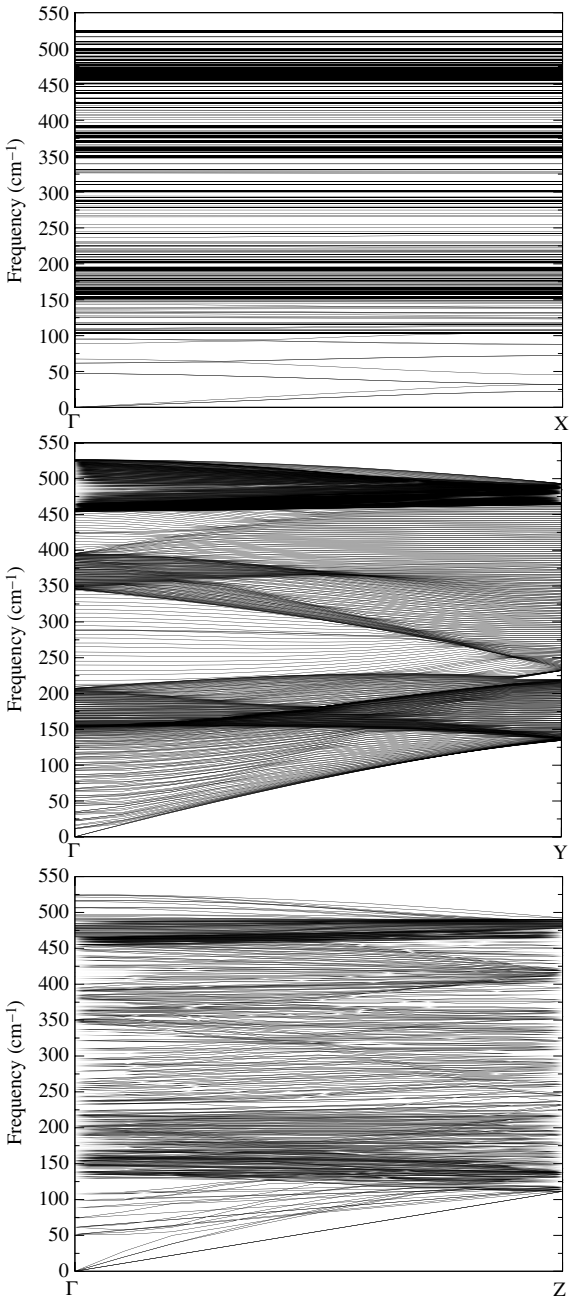

Figure 8. The phonon dispersion curves for an ultrathin silicon nanowire of cross section 0.543 nm × 0.543 nm on a 2.715 nm thick nanoslab. Γ–X is considered perpendicular to the surface of the slab, Γ–Y is perpendicular to the direction of propagation of the wire, and parallel to the direction of propagation of the slab, and Γ–Z is considered in the direction of propagation of both the wire and the slab.

the highest optical mode appears to be dominated by the substrate thickness rather than the wire thickness.

3.4. Behaviour of the highest optical mode

In all stand-alone nanostructures, the frequency ω_{optical} of the highest optical mode shows a marked departure from the highest bulk frequency. This departure becomes more

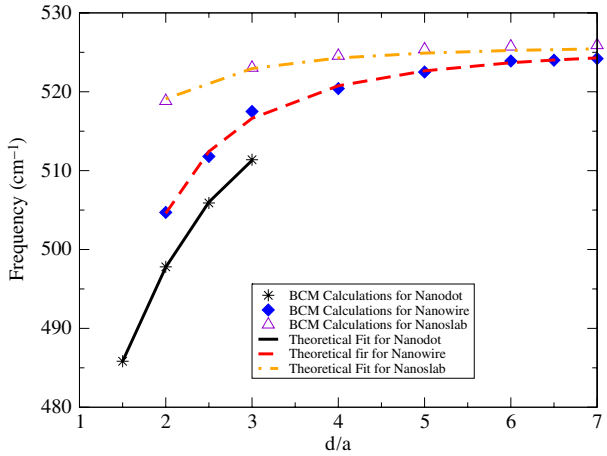

Figure 9. The variation of the highest mode with the size d of the nanostructure. a is the lattice parameter (0.543 nm).

Table 2. Results for the highest and lowest non-zero zone-centre modes for different sizes and dimensionality of nanowire on a substrate. The size d is expressed in units of the cubic lattice constant a of silicon.

Substrate thickness (d/a)	Size of nanowire (d/a)	Size of vacuum (d/a)	ω_σ (cm^{-1})	ω_{optical} (cm^{-1})
1	1	1	117.15	510.45
1	1	2	108.44	510.38
2	1	1	89.81	520.82
2	2	1	74.15	520.35
2	2	2	64.88	520.86
2	2	3	62.90	521.42
3	1	1	72.19	523.45
4	1	1	60.27	524.64
5	1	1	50.88	525.37
5	1	2	46.94	525.41
5	2	2	42.54	525.37
6	1	1	44.22	525.76
6	2	2	37.59	525.73

significant as the number of degrees of quantization increases (i.e. along the sequence nanoslab, nanowire, nanodot). Moreover, as shown in figure 9, for a given number of degree of confinement in a stand-alone nanostructure, ω_{optical} increases with the dimension d of confinement. The size dependence of ω_{optical} was explained for superlattices and thin slabs in the 1980s by Jusserand *et al* [22]. Using the diatomic linear chain model and considering only nearest-neighbour interactions (that is interactions between all atoms within a distance $2a$, where a is the interatomic distance), Jusserand *et al* obtained $\omega_{\text{optical}} \propto 1/d^2$. We will briefly describe their approach and then extend it to obtain expressions for the size dependence of ω_{optical} for the different types of nanostructures considered in this work.

For a diatomic linear chain with masses m_1 and m_2, and interatomic separation a, the dynamical matrix can be expressed as [33] as

$$D = \begin{pmatrix} 2\Lambda_1/m_1 & (-2\Lambda/m_1)\cos qa \\ (-2\Lambda/m_2)\cos qa & 2\Lambda_1/m_2 \end{pmatrix}. \quad (6)$$

In the long wavelength limit we retain only the first-order term

in the expansion of the cosine function and recognize that in the confinement direction $q \propto 1/d$. Hence, solving the dynamical equation $|D - \omega^2 \hat{I}| = 0$ we obtain the result originally shown by Jusserand *et al*:

$$\Delta\omega^2 = \frac{\alpha}{d^2}, \tag{7}$$

where $\Delta\omega^2 = \omega^2_{\text{bulk}} - \omega^2_{\text{optical}}$ with ω_{bulk} being the frequency of the highest optical mode in bulk. This result is applicable for nanoslabs. The above theory can be extended to calculate the effect of quantization in two dimensions (for nanowires) as well as three dimensions (for nanodots).

Application of the model in two dimensions with the same condition as stated previously, namely that we consider interactions between all atoms within the distance $2a$ (where a is the interatomic distance), requires three force constants. Let these be denoted as Λ_1, Λ_2, and Λ_3, where Λ_1 is the m_1–m_2 atomic interaction in the $\langle 100 \rangle$ directions, and Λ_2, and Λ_3 are the m_1–m_1 and m_2–m_2 interactions respectively in the $\langle 110 \rangle$ directions. Here we have considered the nanowire axis along [001], as stated earlier. Setting up a dynamical matrix as before and solving it in a similar manner, it can be shown for confinement in two dimensions that

$$\Delta\omega^2 = \frac{\beta_1}{d^2} + \frac{\beta_2}{d^3}, \tag{8}$$

where β_i are constants.

Similarly, for a nanodot with three-dimensional confinement, we set up a three-dimensional diatomic structure, and use four force constants to account for interatomic interactions up to distances $2a$. The force constant Λ_1 accounts for the nearest-neighbour interactions between m_1 and m_2 in the $\langle 100 \rangle$ directions. Similarly, Λ_2 and Λ_3 account for second-nearest-neighbour interactions (i.e. between m_1–m_1 and m_2–m_2 in the $\langle 110 \rangle$ directions). The fourth force constant, Λ_4 accounts for third-nearest-neighbour interactions (i.e. between m_1 and m_2 in the $\langle 111 \rangle$ directions. From this a dynamical matrix can be set up and solved as above, leading to the result

$$\Delta\omega^2 = \frac{\eta_1}{d^2} + \frac{\eta_2}{d^3} + \frac{\eta_3}{d^4}, \tag{9}$$

where η_i are constants.

Figure 9 shows the fits of these equations to the results from our lattice dynamics calculations using the adiabatic charge model for the three fundamental types of nanostructure. As can be clearly seen, the simple analytical fits are in good agreement with the theoretical results obtained by the theory. Our results can help explain Raman measurements on (ultra)small nanostructures. A suitable extrapolation of our results, using the analytical fits in equations (7)–(9), can be expected to explain Raman measurements on actual nanostructures grown, provided that such samples are clean (i.e. not covered with any protective layers, etc). Our extrapolated results can also be expected to explain differences between grain-like and wire-like behaviour observed in Raman measurements in nanowires [35].

3.5. Intrinsic lifetime of the lowest non-zero mode

It is important to assess the lifetime of the lowest non-zero zone-centre mode, ω_σ, as this mode lies in the acoustic range and can play an important role in heat conduction via electron–phonon interaction as well via phonon–phonon interactions. The basic limiting factors for the intrinsic lifetime of this mode are its decay into lower range of acoustic modes, subject to energy and momentum conservation laws as discussed in section 2.2. Our model leads to three phonon acoustic branches, which are linearly dispersive in the zone-centre region.

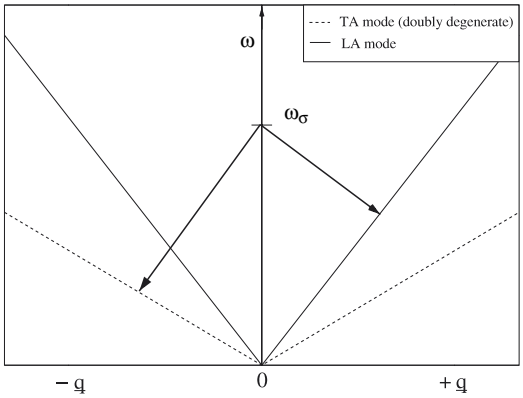

Figure 10. An illustration of the decay of a low-lying zone-centre phonon mode into two linear acoustic modes near the zone centre.

In order to calculate the lifetime, phonon dispersion relations and frequencies of such confined modes in the low energy range are required. These were obtained using the method detailed in section 2.2. As the lowest non-zero confined mode (ω_σ) in the silicon nanostructures are characterized by quite low energies, such modes can be expected to decay into two acoustic modes in the linear part of the dispersion curves, as illustrated in figure 10. The acoustic phonon speeds $c_{s'}$ and $c_{s''}$ were calculated from the linear regime of the dispersion curves. In this work we limit ourselves to the meaningful direction of propagation in the wire and the slab to discuss the behaviour of this mode. The material density ρ is set as 2329 kg m^{-3} for silicon nanostructures. The Grüneisen's constant γ is shown to vary between 0 and 0.5 at low temperatures in bulk silicon [36]. Fabian *et al* [37] have also reported a maximum value of 1.0 for silicon. Hence, based upon this, we decided to take the maximum value for the Grüneisen's constant and set its value to 1.0 for these calculations. This choice provides the minimum value for the lifetime.

We calculated the intrinsic lifetime of this mode for square silicon nanowires ranging from 0.543 to 3.801 nm in thickness. Except for the ultrathin wire (thickness 0.543 nm), the lifetime of the mode increases with wire thickness, as shown in figure 11. This is due to the decrease in frequency of the mode as the wire thickness increases. Equation (4) shows the strong frequency dependence of the relaxation rate (inverse of lifetime) of the mode. The relaxation time of this mode is also highly dependent on the speed of the acoustic modes which it decays into. The variation of the acoustic speeds is shown in table 3. The ultrathin nanowire, with much higher lifetime, does not follow the trend which the thicker wires show of an increase in lifetime with thickness. This is because the phonon spectrum of the ultrathin nanowire is

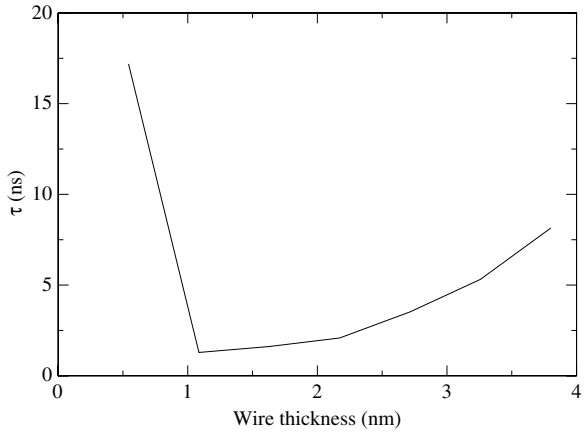

Figure 11. The variation of the lifetime of the lowest non-zero zone-centre confined mode with the thickness of the wire at 300 K.

unusually different and has much higher acoustic velocities than nanowires of other thicknesses.

A comparison of the lifetime results between a nanowire of 1.086 nm × 1.086 nm in size, and a nanoslab of 1.086 nm thickness is shown in figure 12. As can be seen, the nanoslab has longer lifetime than the nanowire. This effect is due to two factors. The acoustic speeds in the nanowire are much higher than in the nanoslab, and ω_σ is higher in the nanowire than in the nanoslab. This trend is expected to continue for all sizes of nanowire and nanoslab as the most dominating factor in the lifetime calculation is the value ω_σ of this mode. Equation (5) shows that ω_σ changes more quickly with d in a nanoslab than in a nanowire. This means that the lifetime of this mode will become much longer than in the wire as slab thickness increases.

Lastly, calculations were performed for an ultrathin nanowire (0.543 nm × 0.543 nm) upon a 2.715 nm thick nanoslab (system A) and for a nanoslab of 2.715 nm thickness (system B). As seen in figure 13, system A has a longer lifetime of its lowest non-zero mode than system B. For these two systems the speeds of the acoustic modes are comparatively the same near the zone centre, suggesting that the zone-centre behaviour of acoustic modes is dominated by the slab, rather than the wire in the case of system A. However, the value

Table 3. The frequencies of the lowest non-zero zone-centre confined mode and the acoustic speeds of the longitudinal and doubly transverse modes for a silicon nanowire of thickness d.

d (nm)	c_L (km s^{-1})	c_T (km s^{-1})	ν_σ (THz)
0.543	24.43	20.27	4.737
1.086	11.86	8.50	3.199
1.629	10.69	7.58	2.628
2.172	9.88	6.67	2.126
2.715	9.10	6.50	1.782
3.258	8.91	6.18	1.520
3.801	8.71	6.11	1.344

of ω_σ is lower in system A compared with system B. This is because whilst confinement effects of the wire may be expected to increase the energy of this mode, the total confinement in the x-direction has decreased, which leads to a decrease in the energy of ω_σ. Thus, as equation (4) shows, the lifetime will increase.

4. Conclusion

Silicon nanostructures have several common features in their lattice dynamics. It can be seen for the ultrasmall case of each structure that all branches except the acoustic are flat and dispersionless regardless of whether the system is 0D, 1D or 2D. As the size of these structures increases, these branches are seen to become dispersive in the direction of propagation. Eventually, as size increases, the branches in the direction of confinement start to follow a similar trend. In all systems studied here, the characteristic lowest non-zero zone-centre mode with frequency ω_σ is calculated and shown to decrease with size of the nanostructure. An analytic fit has been presented for the size variation of this mode for simple structures (dots, wires and slabs). It is also observed that in all systems the highest optical mode is lowered and for simple systems this behaviour can be explained using a simple diatomic model. The calculated results for such variation have been fitted to analytic expressions.

Such features are also observed in the case of nanowires deposited on substrates. For this system the phonon dispersion is in general dominated by the substrate. In particular, the

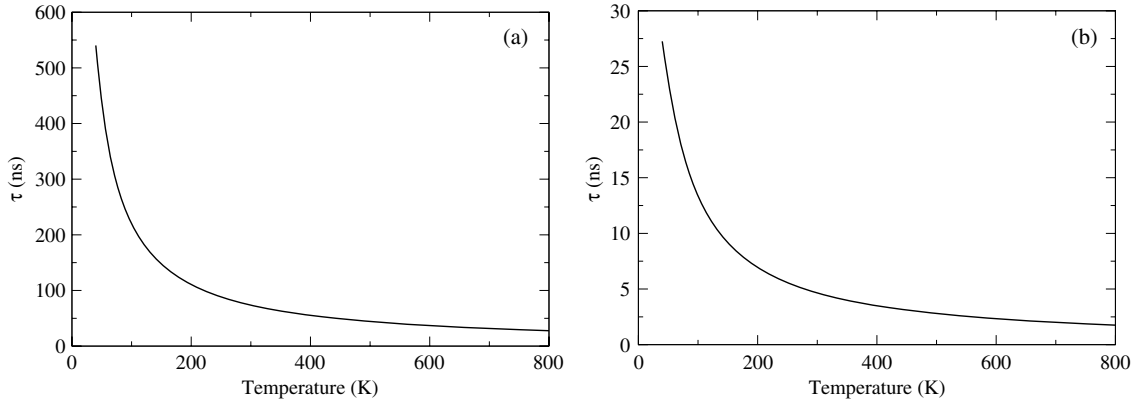

Figure 12. The variation of the lifetime of the lowest non-zero zone-centre confined mode with temperature for (a) a nanoslab of 1.086 nm thickness; (b) a nanowire of cross section 1.086 nm × 1.086 nm.

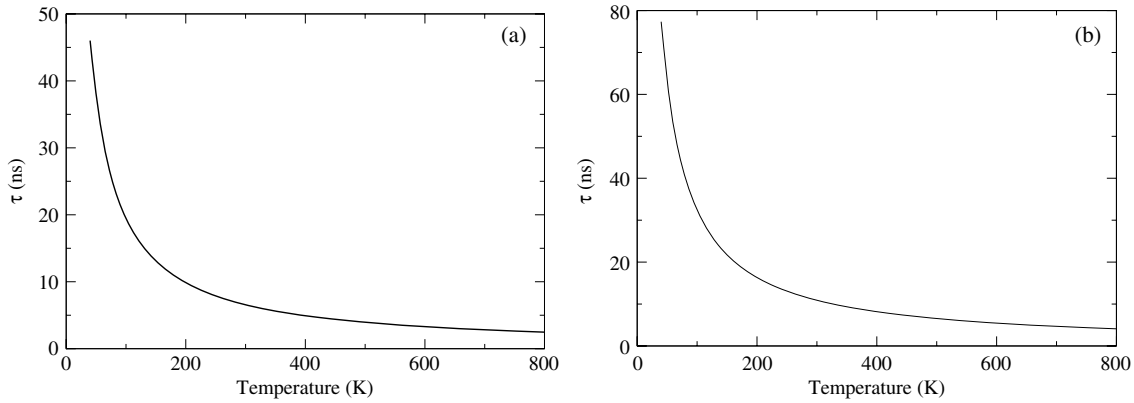

Figure 13. The variation of the lifetime of the lowest non-zero zone-centre confined mode with temperature for (a) a nanoslab of 2.715 nm thickness; (b) a nanowire of cross section 1.086 nm × 1.086 nm grown on a nanoslab of 2.715 nm thickness.

phonon branches in the Γ–Y direction become more dispersive than in the stand-alone nanowire, showing that the addition of the slab reduces quantization in that plane. Also, the frequency ω_σ of a nanowire deposited upon a substrate is lower than that of either of the two stand-alone systems.

Finally, the lifetime of the ω_σ mode undergoing normal processes is shown to be of the order of nanoseconds for all systems. This mode is much longer lived than the optical modes in bulk silicon. Also, from the lattice dynamics calculations, it can be seen that this mode is not flat nor dispersionless except in the smallest cases. Thus, this mode will have an important effect on phonon–electron and phonon–phonon interactions, and will become important in any future calculations of thermal conduction in such systems.

Acknowledgment

SPH gratefully acknowledges financial support from the EPSRC (UK).

References

[1] Han W, Fan S, Li Q and Hu Y 1997 *Science* **277** 1287
[2] Sunkara M, Sharma S, Miranda R, Lian G and Dickey E 2001 *Appl. Phys. Lett.* **79** 1546
[3] Charlier A, McRae E, Charlier M, Spire A and Forster S 1998 *Phys. Rev.* B **57** 6689
[4] Hitosugi T, Hashizume T, Heike S, Kajiyama H, Wada Y, Watanabe S, Hasegawa T and Kitazawa K 1998 *Appl. Surf. Sci.* **130–132** 340
[5] Hofmann S, Ducati C, Neill R J, Piscanec S, Ferrari A C, Geng J, Dunin-Borkowski R E and Robertson J 2003 *J. Appl. Phys.* **94** 6005
[6] Chandreasekar V, Webb R A, Brady M J, Ketchen M B, Gallagher W J and Kleinsasser A 1991 *Phys. Rev. Lett.* **67** 3578
[7] Lorke A, Luyken R J, Govorov A O, Kotthaus J P, Garcia J M and Petroff P M 2000 *Phys. Rev. Lett.* **84** 2223
[8] Iijima S and Ichihashi T 1993 *Nature* **363** 603
[9] Watanabe S, Ono Y, Hashizume T, Wada Y, Yamauchi J and Tsukada M 1995 *Phys. Rev.* B **52** 10768
[10] Stroscio M A and Dutta M 2001 *Phonons in Nanostructures* (Cambridge: Cambridge University Press)
[11] Bannov N, Aristov V, Mitin V and Stroscio M A 1995 *Phys. Rev.* B **51** 9930
[12] Collins P G, Bando H and Zettl A 1998 *Nanotechnology* **9** 153
[13] Cui Y and Lieber M 2001 *Science* **291** 851
[14] Nishiguchi N, Ando Y and Wybourne M N 1997 *J. Phys.: Condens. Matter* **9** 5751
[15] Mingo N and Yang L 2003 *Phys. Rev.* B **68** 245406
[16] Singh R and Prakash S 2003 *Surf. Sci.* **532–535** 780
[17] Stroscio M A, Kim K W, Yu S and Ballato A 1994 *J. Appl. Phys.* **76** 4670
[18] Kanellis G, Morhange J F and Balkanski M 1980 *Phys. Rev.* B **21** 1543
[19] Hu X H and Zi J 2002 *J. Phys.: Condens. Matter* **14** L671
[20] Mingo N 2003 *Phys. Rev.* B **68** 113308
[21] Thonhauser T and Mahan G D 2004 *Phys. Rev.* B **69** 075213
[22] Jusserand B, Paquet D, Mollot F, Alexandre F and Le Roux G 1987 *Phys. Rev.* B **35** 2808
[23] Lamb H 1882 *Proc. London Math. Soc.* **13** 189
[24] Rytov S M 1956 *Akust. Zh.* **2** 71
Rytov S M 1956 *Sov. Phys.—Acoust.* **2** 68 (Engl. Transl.)
[25] Sun C Q, Pam L K, Li C M and Li S 2005 *Phys. Rev.* B **72** 134301
[26] Hepplestone S P and Srivastava G P 2004 *Phys. Status Solidi* c **1** 2617
[27] Hepplestone S P and Srivastava G P 2005 *Appl. Phys. Lett.* **87** 231906
Hepplestone S P and Srivastava G P 2005 *Virtual J. Nanoscale Sci. Technol.* **12** (24)
[28] Weber W 1997 *Phys. Rev.* B **15** 4789
[29] Keating P 1965 *Phys. Rev.* **145** 637
[30] Tütüncü H M and Srivastava G P 1996 *Phys. Rev.* B **53** 15675
[31] Srivastava G P 1999 *Theoretical Modelling of Semiconductor Surfaces* (Singapore: World Scientific)
[32] Ziman J M 1960 *Electrons and Phonons* (Oxford: Oxford University Press, Clarendon)
[33] Srivastava G P 1990 *The Physics of Phonons* (Bristol: Hilger)
[34] Fujii M, Kanzawa Y, Hayashi S and Yamamoto K 1996 *Phys. Rev.* B **54** R8373
[35] Ding W, Li L, Li B and Zhang S 2000 *Chin. Sci. Bull.* **45** 1351
[36] Slack G A and Bartrum S F 1975 *J. Appl. Phys.* **46** 89
[37] Fabian J and Allen P B 1997 *Phys. Rev. Lett.* **79** 1885